Analysis and Suppression of the Circulating Current Influence in the Input-Series Auxiliary Power Supply for High-Input-Voltage Applications

Tao Meng, *Member, IEEE*, Hongqi Ben, Yilin Song, and Chunyan Li

***Abstract*—The input-series converters based on transformer integration have the advantages of active input voltage sharing (IVS) and simplicity of the whole system, which are suitable for the high-input voltage multiple-output applications. However, due to the parameters error in each series module, the circulating current occurs among the series modules during the active IVS process. Aiming at this type input-series two-transistor flyback converter, the mechanism and influence of the circulating current in each series module are analyzed. On this basis, according to the characteristics of the peak current mode control scheme adopted in this converter, a suppression strategy is proposed, by which influence of the circulating current on the operational stability of the converter under the light load conditions can be eliminated. Finally, based on the simulating results, the experimental study has been done on a 60-W experimental prototype composed of three series modules, and the theoretical analysis and the proposed suppression strategy have been verified by the experimental results.**

***Index Terms*—Circulating current, input-series, multiple-output auxiliary power supply, transformer integration, two-transistor flyback.**

I. Introduction

THE input-series scheme is an effective scheme to reduce the voltage stress of each device in the converters with high-input voltage. For the input-series converters, the most important issue is to achieve the voltage or current sharing. For example, for the input-series output-parallel (ISOP) converters, the input voltage sharing (IVS) and output current sharing must be ensured, and for the input-series output-series converters, in addition to the IVS, the output voltage sharing should also be achieved [1]–[4]. To realize voltage or current sharing of the

Manuscript received July 28, 2018; revised September 12, 2018; accepted October 11, 2018. Date of publication October 15, 2018; date of current version May 2, 2019. This work was supported in part by the National Natural Science Foundation of China under Grant 51677056, in part by the Natural Science Foundation of Heilongjiang Province under Grant E2016052, in part by the Postdoctoral Science Foundation of Heilongjiang Province under Grant LBH-Q17145, in part by the Heilongjiang University Science Foundation for Distinguished Young Scholars under Grant JCL201604, and in part by the Heilongjiang University Fundamental Research Funds for the Heilongjiang Province Universities under Grant RCYJTD201802. Recommended for publication by Associate Editor I. Barbi. *(Corresponding author: Tao Meng.)*

T. Meng, Y. Song, and C. Li are with the School of Mechanical and Electrical Engineering, Heilongjiang University, Harbin 150080, China (e-mail:

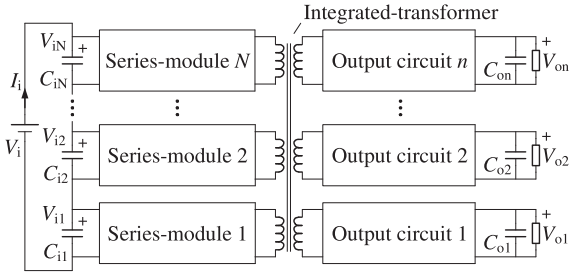

Fig. 1. Basic configuration of the input-series converter based on transformer integration.

The typical investigations of the interleaved operating converters are as follows. In [23]–[25], the input-series converters composed of two forward series modules are presented. Due to the interleaved operation of these converters, the magnetic core utilization of each integrated transformer has been improved. However, number of the series modules cannot be increased arbitrarily due to the interleaved operation of the two series modules. Therefore, these converters cannot be very suitable for the high-input voltage applications.

The typical investigations of the synchronous operating converters are as follows. In [26]–[29], the input-series converters based on the full-bridge and half-bridge topologies are presented. In these converters, the series modules operate synchronously and active IVS can be achieved for each series module. Generally, these converters are designed for the medium or high power applications. In [30]–[32], the input-series flyback and forward converters are investigated. In these converters, active IVS can also be ensured with the synchronous operating of each series module. Compared to the full-bridge and half-bridge converters, these converters are much more suitable for the multiple-output low-power applications. Among these flyback and forward converters, structures of the flyback converters in [30] and [31] are simpler than that of the forward converter in [32], where the single-switch flyback converter in [30] has the simplest structure, and the flyback converters are more suitable for the low-power applications. Furthermore, due to the much lower voltage stress of the power switches in each series module, the two-transistor flyback and forward converters in [31] and [32] are more suitable for the high-input voltage applications.

For the above input-series synchronous operating converters, a good IVS performance has been ensured in each series module. However, the input voltage difference cannot be eliminated completely due to the parameters error of each series module, so the circulating current occurs in each series module, by which the operational stability of the converter will be affected. Therefore, the circulating current problem of these converters is investigated in this paper. As the input voltage increases or the conversion power decreases, the circulating current problem will be more serious in each series module, which has been analyzed and verified in this paper. Therefore, the investigation of this paper is aiming at the input-series flyback and forward converters in [30]–[32], and the main analysis is based on the input-series two-transistor flyback converter in [31], in which the circulating current problem is more serious than the other converters because of its high-input voltage and low-power applications.

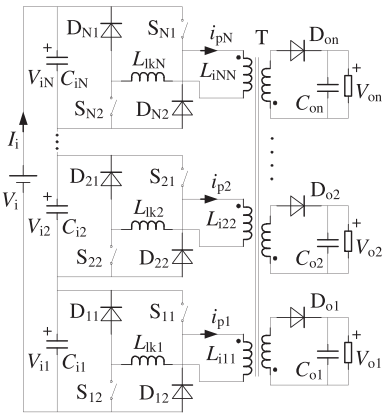

Fig. 2. Input-series two-transistor flyback converter.

This paper is organized as follows. In Section II, the circulating current is analyzed based on the input-series two-transistor flyback converter. In Section III, influence of the circulating current is discussed, and the suppression strategy is proposed. The theoretical analysis is verified by the simulating and experimental results in Section IV, and the conclusions are given in Section V. Furthermore, the circulating current in the input-series single-switch flyback converter and the input-series forward converter are presented briefly in the "Appendix" section.

II. Circulating Current of the Input-Series Two-Transistor Flyback Converter

A. Input-Series Two-Transistor Flyback Converter

The input-series two-transistor flyback converter is shown in Fig. 2, where there are N ($N \geq 1$) series modules and n ($n \geq 1$) output circuits. In various series modules, there are the same power devices and parameters, such as the input capacitances ($C_{i1} = C_{i2} = \cdots = C_{\mathrm{iN}}$), the switches ($\mathrm{S}_{11}$, S_{12}, S_{21}, S_{22}, …, $\mathrm{S}_{\mathrm{N}1}$, $\mathrm{S}_{\mathrm{N}2}$), the diodes (D_{11}, D_{12}, D_{21}, D_{22}, …, $\mathrm{D}_{\mathrm{N}1}$, $\mathrm{D}_{\mathrm{N}2}$), and the primary inductances ($L_{i11} = L_{i22} = \cdots = L_{i\mathrm{NN}}$) of the integrated-transformers T. In this converter, the switches in different series modules are operating synchronously, active IVS can be realized with the help of the integrated transformer, and the IVS performance cannot be affected by its output circuits.

Active IVS of this converter can be realized, but the circulating current appears in each series module during the IVS process. To simplify the circulating current analysis, it is assumed: 1) two series modules ($N = 2$) are considered and 2) all devices are ideal, so the error of parameters in the two series modules is ignored.

During one switching period, active IVS processes of this converter appear in the following two stages: In stage 1 (t_0–t_1), all of the switches are turned ON, and the primary inductors of the integrated transformer are charged by the input source, and in stage 2 (t_1–t_2), all of the switches are turned OFF, energy of the primary inductors of the integrated transformer has been transferred to the secondary inductors, and energy of the leakage

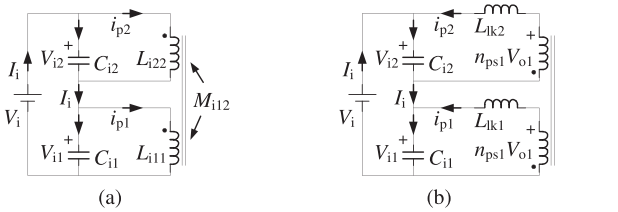

Fig. 3. Equivalent circuits in primary side of the flyback integrated transformer. (a) Stage 1. (b) Stage 2.

inductor is transferred to the input side of each series module. Therefore, the circulating current is analyzed in the above two stages, respectively.

B. Analysis of the Circulating Current in Stage 1

In stage 1, the flyback integrated transformer is equal to a coupled-inductor, and the equivalent circuit of its primary side is shown in Fig. 3(a), where L_{i11}, L_{i22} ($L_{i11} = L_{i22}$) are the self-inductances, and M_{i12} is the mutual inductance. So, it can be obtained that

$$\begin{cases} V_{i1}(t) = L_{i11}\dfrac{di_{p1}(t)}{dt} + M_{i12}\dfrac{di_{p2}(t)}{dt} \\ V_{i2}(t) = L_{i22}\dfrac{di_{p2}(t)}{dt} + M_{i12}\dfrac{di_{p1}(t)}{dt} \end{cases} \tag{1}$$

$$M_{i12} = k\sqrt{L_{i11}L_{i22}} = kL_{i11} \tag{2}$$

where k ($0 \le k \le 1$) is the coupling coefficient.

It is assumed that the input voltage difference (ΔV_i) appears at t_0, and then the active IVS process occurs after t_0. So, the following relationships can be obtained: before t_0, $I_i = i_{p1} = i_{p2}$, $V_{i1} = V_{i2} = V_i/2$, and at t_0, $I_i = i_{p1} = i_{p2}$, $V_{i1} = V_i/2 + \Delta V_i$, $V_{i2} = V_i/2 - \Delta V_i$, where $\Delta V_i(t_0) > 0$. After t_0, the input voltage difference can be estimated from the analysis in [31] as

$$\Delta V_i(t - t_0) = \Delta V_i(t_0)\cos\frac{t - t_0}{\sqrt{(1-k)L_{i11}C_{i1}}}. \tag{3}$$

It can be seen that if the input voltage difference appears at t_0, a high frequency resonance will occur. Because of the internal resistance in each series module, the resonant amplitude decreases in each period, and active IVS of each series module will be achieved immediately after t_0. This IVS process is shown in Fig. 4(a).

For the two input capacitors (C_{i1} and C_{i2}), it can be obtained after t_0 that

$$\begin{cases} C_{i1}\dfrac{dV_{i1}(t-t_0)}{dt} = I_i(t-t_0) - i_{p1}(t-t_0) \\ C_{i2}\dfrac{dV_{i2}(t-t_0)}{dt} = I_i(t-t_0) - i_{p2}(t-t_0). \end{cases} \tag{4}$$

It can be obtained from (4) that

$$i_{p1}(t-t_0) + i_{p2}(t-t_0) = 2I_i(t-t_0) \tag{5}$$

$$i_{p1}(t-t_0) - i_{p2}(t-t_0) = -2C_{i1}\frac{d\Delta V_i(t-t_0)}{dt}. \tag{6}$$

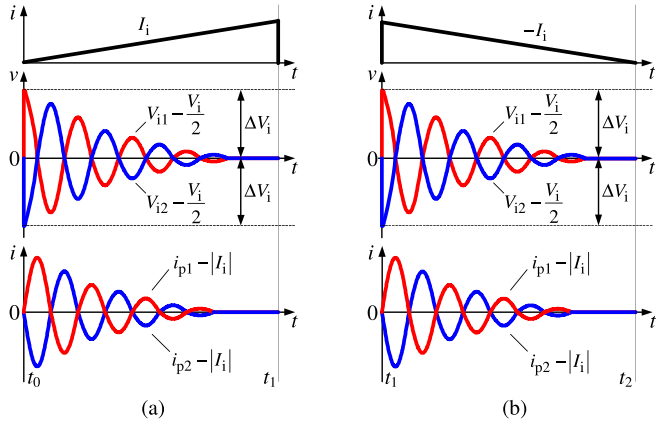

Fig. 4. Input voltage difference and the circulating current during the active IVS processes. (a) Stage 1. (b) Stage 2.

Therefore, after t_0, the expressions of i_{p1} and i_{p2} can be obtained from (3), (5), and (6)

$$\begin{cases} i_{p1}(t-t_0) = I_i(t-t_0) + \Delta V_i(t_0)\sqrt{\dfrac{C_{i1}}{(1-k)L_{i11}}} \\ \qquad \sin\dfrac{t-t_0}{\sqrt{(1-k)L_{i11}C_{i1}}} \\ i_{p2}(t-t_0) = I_i(t-t_0) - \Delta V_i(t_0)\sqrt{\dfrac{C_{i1}}{(1-k)L_{i11}}} \\ \qquad \sin\dfrac{t-t_0}{\sqrt{(1-k)L_{i11}C_{i1}}} \end{cases} \tag{7}$$

where I_i can be calculated as follows:

$$I_i(t-t_0) = I_i(t_0) + \int_{t_0}^{t}\frac{V_i}{2(1+k)L_{i11}}dt. \tag{8}$$

C. Analysis of the Circulating Current in Stage 2

In stage 2, the equivalent circuit in primary side of the flyback integrated transformer is shown in Fig. 3(b), where L_{LK1} and L_{LK2} are the equivalent leakage inductors. In this stage, the energy in primary side of the integrated transformer has been transferred to the secondary side, and the voltage of each primary winding is fixed at $n_{ps1}\ V_{o1}$ (n_{ps1} is the turn ratio of the integrated transformer, which is equal to the turn ratio between the primary winding and the secondary winding for the output circuit of V_{o1}).

It is assumed that the input voltage difference (ΔV_i) appears at t_1, and then the active IVS process occurs after t_1. So, the following relationships can be obtained: before t_1, $-I_i = i_{p1} = i_{p2}$, $V_{i1} = V_{i2} = V_i/2$, and at t_1, $-I_i = i_{p1} = i_{p2}$, $V_{i1} = V_i/2 + \Delta V_i$, $V_{i2} = V_i/2 - \Delta V_i$, where $\Delta V_i(t_1) > 0$. After t_1, the input voltage difference can be estimated from the analysis in [31] as

$$\Delta V_i(t - t_1) = \Delta V_i(t_1)\cos\frac{t - t_1}{\sqrt{(1-k)L_{i11}C_{i1}}}. \tag{9}$$

It can be seen that if the input voltage difference appears at t_1, a high frequency resonance will also occur, and as shown in

Fig. 4(b), the active IVS of each series module will be achieved immediately after t_1.

For the two input capacitors (C_{i1} and C_{i2}), it can be obtained after t_1 that

$$\begin{cases} C_{i1}\dfrac{dV_{i1}(t-t_1)}{dt} = I_i(t-t_1) + i_{p1}(t-t_1) \\ C_{i2}\dfrac{dV_{i2}(t-t_1)}{dt} = I_i(t-t_1) + i_{p2}(t-t_1). \end{cases} \tag{10}$$

It can be obtained from (10) that

$$i_{p1}(t-t_1) + i_{p2}(t-t_1) = -2I_i(t-t_1) \tag{11}$$

$$i_{p1}(t-t_1) - i_{p2}(t-t_1) = 2C_{i1}\frac{d\Delta V_i(t-t_1)}{dt}. \tag{12}$$

Therefore, after t_1, the following expressions of i_{p1} and i_{p2} can be obtained from (9), (11), and (12):

$$\begin{cases} i_{p1}(t-t_1) = -I_i(t-t_1) - \Delta V_i(t_1)\sqrt{\dfrac{C_{i1}}{(1-k)L_{i11}}} \\ \qquad \sin\dfrac{t-t_1}{\sqrt{(1-k)L_{i11}C_{i1}}} \\ i_{p2}(t-t_1) = -I_i(t-t_1) + \Delta V_i(t_1)\sqrt{\dfrac{C_{i1}}{(1-k)L_{i11}}} \\ \qquad \sin\dfrac{t-t_1}{\sqrt{(1-k)L_{i11}C_{i1}}} \end{cases} \tag{13}$$

where I_i can be calculated as follows:

$$I_i(t-t_1) = I_i(t_1) + \int_{t_1}^{t}\frac{V_i - 2nV_{o1}}{L_{lk1}+L_{lk2}}dt. \tag{14}$$

From (7), (8), (13), and (14), it can be seen that if the input voltage difference appears in these two stages, the circulating current appears in each series module during the IVS processes, as shown in Fig. 4. Here, it is considered that the converter operates in discontinuous current mode. If the converter operates in continuous current mode, the circulating current varying is similar, which is not given again. It can be concluded that: 1) due to the input voltage difference, the circulating current appears in each series module during the IVS processes and 2) the circulating current value will increase as the input voltage difference increases.

III. Analysis and Suppression of the Circulating Current Influence

A. Analysis of the Circulating Current Influence

The circulating current in each series module is caused by the input voltage difference. In ideal condition, the series modules have the same parameters, and the series modules are operating at the same time, so there is no voltage difference appearing in each series module. However, synchronous operating of the switches cannot be achieved absolutely, which is due to the parameter errors of the switches and their driving circuits. As a result, there is voltage difference appearing in each series module. The input voltage difference is analyzed as follows, where it is also considered that "$N = 2$," and it is defined that the maximum turning ON and OFF time difference of the switches in different series modules are ΔT_0 and ΔT_1, respectively, and the turning ON or OFF difference of the switches in the same series module is not considered.

It is assumed that: before t_0, there is no input voltage difference in each series module ($\Delta V_i = 0$, $V_{i1} = V_i/2 + \Delta V_i = V_i/2$, and $V_{i2} = V_i/2 - \Delta V_i = V_i/2$). If S_{21} and S_{22} are turned ON at t_0, S_{11} and S_{12} are turned ON at $t_0 + \Delta T_0$, and then during the time phase t_0 to $t_0 + \Delta T_0$, $i_{p1} = 0$, V_{i1} increases, V_{i2} decreases, the input voltage difference appears, and it can be obtained from Fig. 3(a)

$$\Delta V_i(t-t_0) = \frac{V_i}{2} - L_{i22}\frac{di_{p2}(t-t_0)}{dt} \tag{15}$$

$$C_{i1}\frac{d\Delta V_i(t-t_0)}{dt} = I_i(t-t_0) = i_{p2}(t-t_0) - I_i(t-t_0). \tag{16}$$

From (15) and (16), the following equation can be obtained:

$$\frac{d^2\Delta V_i(t-t_0)}{dt^2} + \frac{\Delta V_i(t-t_0)}{2L_{i11}C_{i1}} = \frac{V_i}{4L_{i11}C_{i1}}. \tag{17}$$

The solution of (17) can be calculated as follows:

$$\Delta V_i(t-t_0) = \frac{V_i}{2}\left(1 - \cos\frac{t-t_0}{\sqrt{2L_{i11}C_{i1}}}\right) + I_i(t_0)\sqrt{\frac{2L_{i11}}{C_{i1}}}\sin\frac{t-t_0}{\sqrt{2L_{i11}C_{i1}}}. \tag{18}$$

It is assumed that: Before t_1, there is no input voltage difference in each series module ($\Delta V_i = 0$, $V_{i1} = V_i/2 + \Delta V_i = V_i/2$, and $V_{i2} = V_i/2 - \Delta V_i = V_i/2$). If S_{11} and S_{12} are turned OFF at t_1, S_{21} and S_{22} are turned OFF at $t_1 + \Delta T_1$, and then during the time phase t_1 to $t_1 + \Delta T_1$, $i_{p1} = 0$, V_{i1} increases, V_{i2} decreases, the input voltage difference appears, and it can be obtained from Fig. 3(a)

$$\Delta V_i(t-t_1) = \frac{V_i}{2} - L_{i22}\frac{di_{p2}(t-t_1)}{dt} \tag{19}$$

$$C_{i1}\frac{d\Delta V_i(t-t_1)}{dt} = I_i(t-t_1) = i_{p2}(t-t_1) - I_i(t-t_1). \tag{20}$$

From (19) and (20), the following equation can be obtained:

$$\frac{d^2\Delta V_i(t-t_1)}{dt^2} + \frac{\Delta V_i(t-t_1)}{2L_{i11}C_{i1}} = \frac{V_i}{4L_{i11}C_{i1}}. \tag{21}$$

The solution of (21) can be calculated as follows:

$$\Delta V_i(t-t_1) = \frac{V_i}{2}\left(1 - \cos\frac{t-t_1}{\sqrt{2L_{i11}C_{i1}}}\right) + I_i(t_1)\sqrt{\frac{2L_{i11}}{C_{i1}}}\sin\frac{t-t_1}{\sqrt{2L_{i11}C_{i1}}}. \tag{22}$$

This converter is often used as the low-power auxiliary power supply with high-input voltage. Therefore, after t_0 or t_1, the following input voltage difference can be estimated from (18) and (22):

$$\Delta V_i(t-t_{0/1}) \approx \frac{V_i}{2}\left(1 - \cos\frac{t-t_{0/1}}{\sqrt{2L_{i11}C_{i1}}}\right). \tag{23}$$

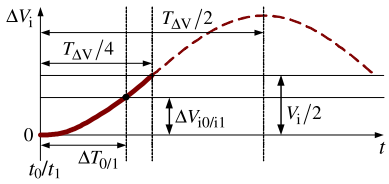

Fig. 5. Varying curve of the input voltage difference.

Therefore, after t_0 or t_1, the varying curve of ΔV_i is obtained in Fig. 5. Because of $\Delta V_i \le V_i/2$, the effective part of this varying curve is the first one-fourth resonant period $T_{\Delta V}$. It can be seen that: 1) ΔV_i will increase as ΔT_0 (or ΔT_1) increases and 2) for the constant values of ΔT_0 (or ΔT_1), ΔV_i will decrease as $T_{\Delta V}$ increases.

In (23), the resonant period can be calculated as

$$T_{\Delta V} = 2\pi\sqrt{2L_{i11}C_{i1}}. \tag{24}$$

From (7), (13), (23), and (24), amplitude of the circulating current (ΔI_p) can be calculated as

$$\Delta I_p = V_i\left(\sin\frac{\pi\Delta T_{0/1}}{T_{\Delta V}}\right)^2\sqrt{\frac{C_{i1}}{(1-k)L_{i11}}}. \tag{25}$$

From (25), it can be seen that: 1) ΔI_p will increase as ΔT_0 (or ΔT_1) increases and 2) for the constant values of ΔT_0 (or ΔT_1), ΔI_p will increase as V_i increases. Generally, the turning ON or OFF difference of the switches is very small, which is much smaller than resonant period $(\Delta T_{0/1} << T_{\Delta V})$.

It can be obtained from the mathematical knowledge that

$$\lim_{x\to 0}\frac{\sin x}{x} = 1. \tag{26}$$

Therefore, amplitude of the circulating current (ΔI_p) can be estimated from (24)–(26) that

$$\Delta I_p \approx V_i\left(\frac{2\pi\Delta T_{0/1}}{T_{\Delta V}}\right)^2\sqrt{\frac{C_{i1}}{(1-k)L_{i11}}} = \frac{V_i(\Delta T_{0/1})^2}{8L_{i11}\sqrt{(1-k)L_{i11}C_{i1}}}. \tag{27}$$

It can be seen from (27) that: ΔI_p will decrease as L_{i11} (or C_{i1}) increases. Generally, for the flyback converter, the primary inductance of its transformer cannot be changed arbitrarily. Therefore, in this converter, an optimal design of C_{i1} can be implemented to reduce the circulating current. For example, if ΔI_p is limited within $5\%\, I_i(t_1)$ during each switching period, the design required of C_{i1} can be obtained from (27) as

$$\sqrt{C_{i1}} \ge \frac{5V_i(\Delta T_{0/1})^2}{2I_i(t_1)L_{i11}\sqrt{(1-k)L_{i11}}} \tag{28}$$

where $I_i(t_1)$ can be calculated from (8).

In this converter, the circulating current is caused by the input voltage difference. Because the asynchronous operating of each series module cannot be avoided, the input voltage difference cannot be eliminated. Therefore, the circulating current can only be reduced through the optimal design of each series module, but cannot be eliminated completely.

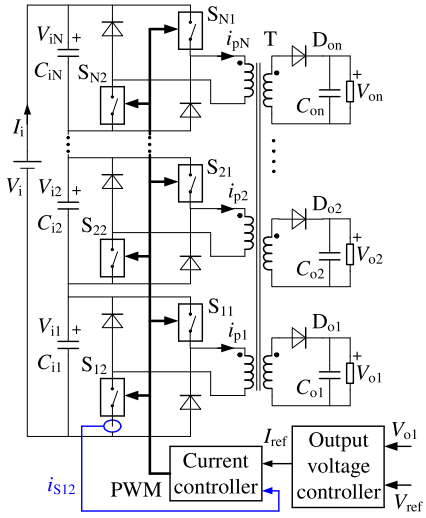

Fig. 6. Control scheme of the input-series two-transistor flyback converter.

It can be seen from (25) and (27) that: Amplitude of the circulating current (ΔI_p) has almost no relationship with the conversion power (P_o) of the converter. As P_o decreases, I_i will decrease accordingly, but ΔI_p would not, so the proportion of the circulating current in the primary current of the integrated transformer will increase as P_o decreases. Therefore, the circulating current cannot be ignored when the converter operates under the light load conditions, even if the circulating current has been reduced by the optimal design of each series module.

For the input-series two-transistor flyback converter, the basic control scheme is shown in Fig. 6 [31], where a peak current mode controller is adopted in the control circuit, the voltage V_{o1} and current i_{S12} are sampled as the outer and inner signals respectively, and a regulated pulsewidth modulation (PWM) signal is output from the controller for the driving circuits of the switches. From the circulating current analysis, it can be seen that there is also circulating current appearing in the inner current signal (i_{S12}) of the controller. After the optimal design of each series module, the proportion of the circulating current is very small in the inner current signal. However, when the converter operates under the light load conditions, the proportion of the circulating current will increase in the inner current signal, as a result, operational stability of the converter will be affected. Therefore, the circulating current should be removed from the inner current signal of the controller to improve the operational stability of the converter under the light load conditions.

B. Suppression Strategy of the Circulating Current Influence

For the input-series two-transistor flyback converter with *N* series modules, it can be obtained from (5) that

$$\sum_{m=1}^{N} i_{\mathrm{pm}}(t-t_0) = NI_i(t-t_0). \tag{29}$$

Moreover, in stage 1, the current of each switch is equal to the primary current of the integrated transformer. Therefore, it

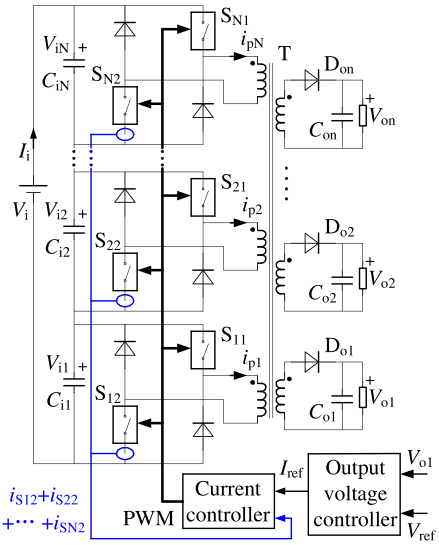

Fig. 7. Suppression strategy of the circulating current influence.

can also be obtained that

$$\sum_{m=1}^{N} i_{Sm1}(t-t_0) = \sum_{m=1}^{N} i_{Sm2}(t-t_0) = NI_i(t-t_0). \quad (30)$$

From (8), (29), and (30), it can be obtained that: In stage 1, whether there is input voltage difference or not in each series module, there will be no circulating current in the sum current $i_{\mathrm{p}1} + i_{\mathrm{p}2} + \cdots + i_{\mathrm{pN}}$, $i_{\mathrm{S}11} + i_{\mathrm{S}21} + \cdots + i_{\mathrm{SN}1}$, and $i_{\mathrm{S}12} + i_{\mathrm{S}22} + \cdots + i_{\mathrm{SN}2}$, and these current waveforms (NI_{i}) are the same as that of I_{i} in Fig. 4(a). Therefore, the sum current $i_{\mathrm{S}12} + i_{\mathrm{S}22} + \cdots + i_{\mathrm{SN}2}$ can be sampled as the inner current signal of the controller instead of only the current $i_{\mathrm{S}12}$, as shown in Fig. 7. After this improvement, there is no circulating current in the inner current signal of the controller, so the operational stability of the converter under the light load conditions would not be affected by the circulating current appearing in each series module.

IV. Simulating and Experimental Verifications

To verify the theoretical analysis, simulating study has been implemented. Furthermore, experiment has been done on a laboratory-made prototype of the input-series two-transistor flyback converter. This prototype was first built for the experimental verification in [31], where the control scheme in Fig. 6 is adopted. In this experiment, the proposed suppression strategy in Fig. 7 is adopted. As shown in Fig. 8, the sum current ($i_{\mathrm{S}12} + i_{\mathrm{S}22} + i_{\mathrm{S}32}$) is sampled to be the inner current signal (i_S) of the controller by a current transformer, which is mainly made up of an annular magnetic core with the winding rounded.

The main parameters of this experimental prototype are: 1) V_i: 1000–2200 Vdc, and $N = 3$; 2) $V_{o1} = V_{o2} = 24$ V, $I_{o1} = 1.5$ A, $I_{o2} = 1$ A, and $P_{o\max} = 60$ W; 3) the switching frequency is 50 kHz; 4) $L_{i11} = L_{i22} = L_{i33} = 2.9$ mH, and $n_{ps1} = 11$; and 5) $C_{o1} = C_{o2} = 1000$ μF.

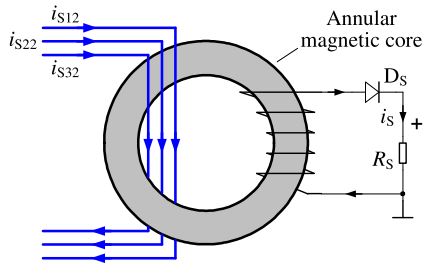

Fig. 8. Inner current sampling method based on a current transformer.

A. Simulating Verifications

Fig. 9 shows the simulating results of this converter, which are the supplements to the following experimental results. In these simulating results, only two series modules ($N = 2$) are considered, the input voltage V_i is 700 V, the output power P_o is 60 W, and the key parameters in each series module are the same as those in the experimental prototype. It can be seen that there is circulating current in the current i_{p1} and i_{p2}, but there is no circulating current in the sum current $i_{p1} + i_{p2}$.

In Fig. 9, the simulating waveforms are obtained when $\Delta T_0 = 0.5$ μs and $\Delta T_0 = 1$ μs, $C_{i1} = C_{i2} = 0.01$ μF and $C_{i1} = C_{i2} = 0.02$ μF, respectively. From Fig. 9(a) and (b), it can be seen that as the turning on time difference (ΔT_0) increases, the input voltage difference increases, and the circulating current value also increases. From Fig. 9(b) and (c), it can be seen that as C_{i1} and C_{i2} increase, the input voltage difference decreases, and the circulating current value also decreases.

B. Experimental Verifications

According to the analyzing and simulating results, to reduce the circulating current and protect the experimental prototype, the input capacitor ($C_{i1} = C_{i2} = C_{i3} = 0.1$ μF) is adopted in each series module in this experiment. The experimental results of this prototype under heavy load conditions have been presented in [31], which are not given again. Here the experimental results of the prototype under the light load conditions are mainly given and discussed, which are aiming at the circulating current of each series module.

Figs. 10–14 show the experimental waveforms when $V_i \approx 1050$ V and $V_i \approx 2100$ V, $P_o = 16$ W and $P_o = 3.84$ W, respectively. In the following current waveforms, the current spike is mainly caused by the charging of the parasitic capacitors in the circuit and the transformer when the switches are turned ON, which will increase as the input voltage increases. This current spike problem also exists in the other conventional flyback converters, so it is not discussed here.

Figs. 10 and 11 show the driving and current waveforms of the switches S_{12}, S_{22}, S_{32} when $P_o = 16$ W. It can be seen that: The three current waveforms are different, there is circulating current in the current waveform of each switch, and the circulating current in each switch (or the current difference) becomes more obvious as the input voltage increases.

Figs. 12 and 13 show the driving and current waveforms of the switches S_{12}, S_{22}, S_{32} when $P_o = 3.84$ W. It can also be

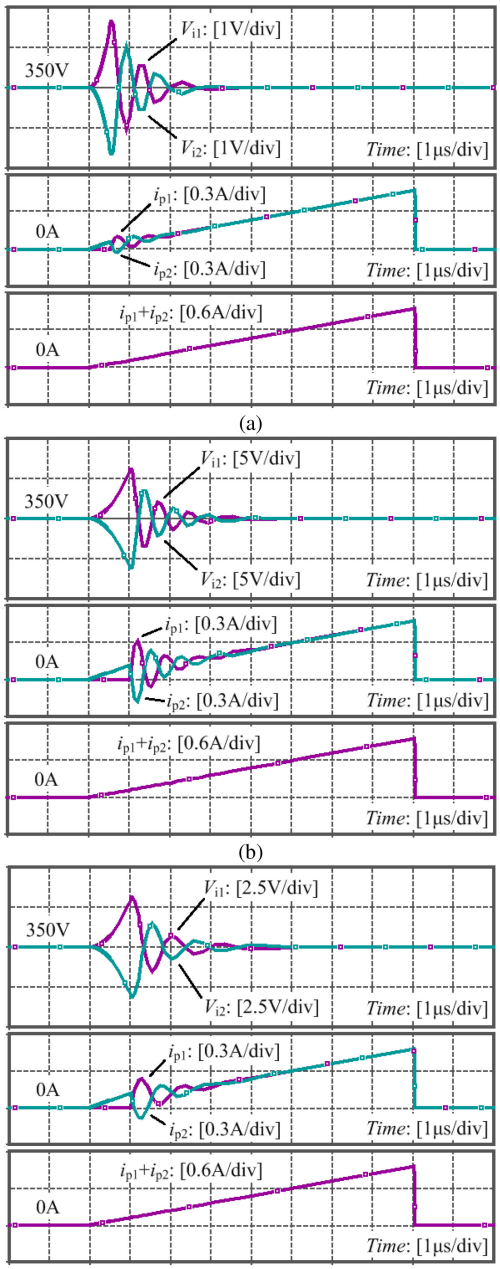

Fig. 9. Simulating waveforms of V_{i1}, V_{i2}, i_{p1}, i_{p2}, and $i_{p1} + i_{p2}$. (a) When $\Delta T_0 = 0.5$ μs, and $C_{i1} = C_{i2} = 0.01$ μF. (b) When $\Delta T_0 = 1$ μs, and $C_{i1} = C_{i2} = 0.01$ μF. (c) When $\Delta T_0 = 1$ μs, and $C_{i1} = C_{i2} = 0.02$ μF.

seen that: The three current waveforms are different, there is circulating current in the current waveform of each switch, and the circulating current in each switch (or the current difference) becomes more obvious as the input voltage increases. Furthermore, compared to the experimental results in Figs. 10 and 11, another conclusion can also be obtained that: the circulating current problem will be more serious as the output power of the converter decreases.

Fig. 14 shows the driving waveforms of S_{12} and the sum current waveforms of $i_{S12} + i_{S22} + i_{S32}$ when $P_o = 16$ W and $P_o = 3.84$ W, $V_i \approx 1050$ V and $V_i \approx 2100$ V, respectively. It

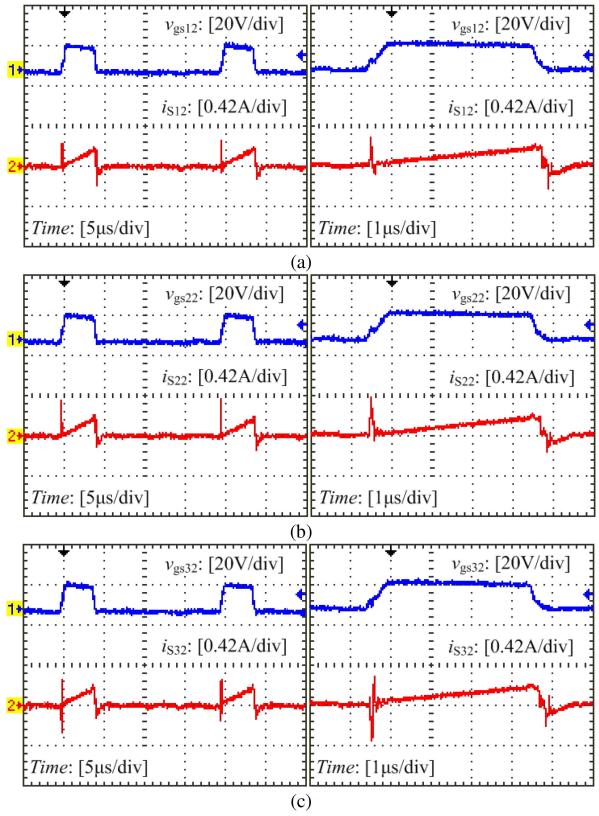

Fig. 10. Driving and current of the switches when $V_i \approx 1050$ V and $P_o = 16$ W. (a) Waveforms of S_{12}. (b) Waveforms of S_{22}. (c) Waveforms of S_{32}.

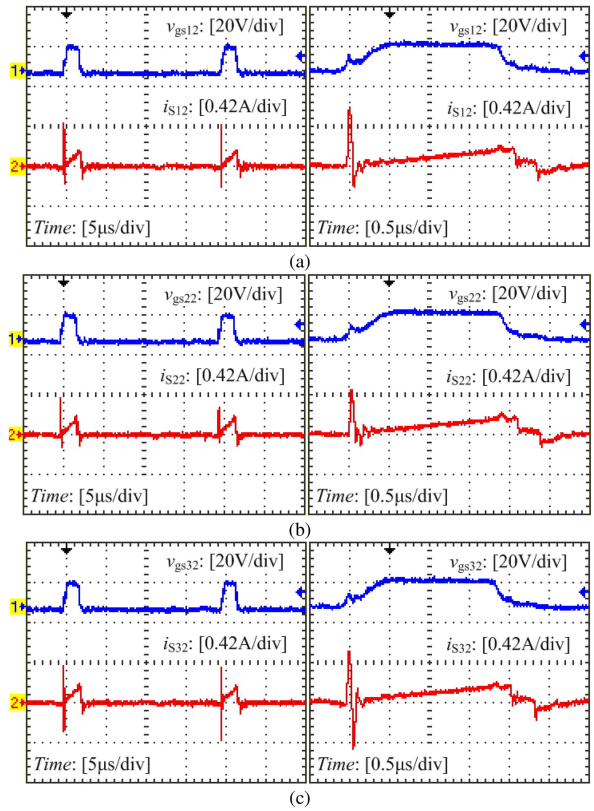

Fig. 11. Driving and current of the switches when $V_i \approx 2100$ V and $P_o = 16$ W. (a) Waveforms of S_{12}. (b) Waveforms of S_{22}. (c) Waveforms of S_{32}.

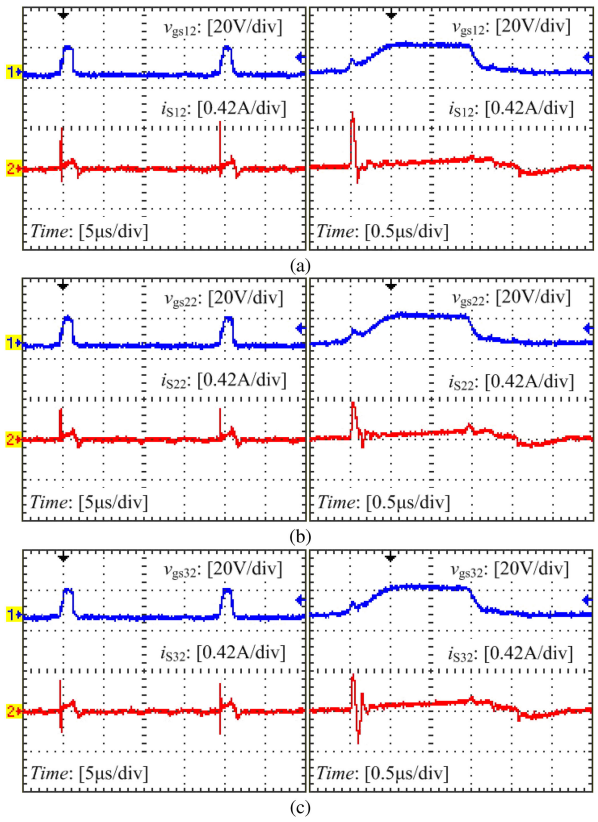

Fig. 12. Driving and current of the switches when $V_i \approx 1050$ V and $P_o = 3.84$ W. (a) Waveforms of S_{12}. (b) Waveforms of S_{22}. (c) Waveforms of S_{32}.

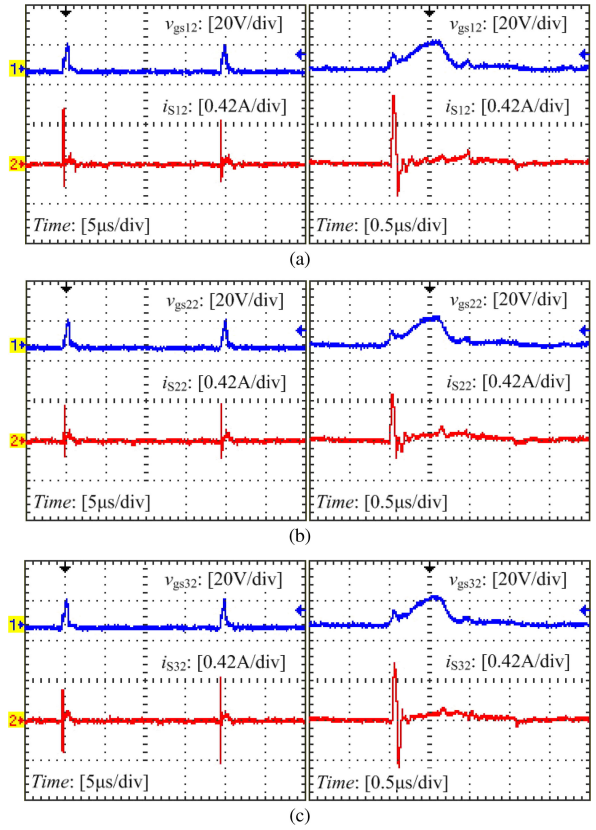

Fig. 13. Driving and current of the switches when $V_i \approx 2100$ V and $P_o = 3.84$ W. (a) Waveforms of S_{12}. (b) Waveforms of S_{22}. (c) Waveforms of S_{32}.

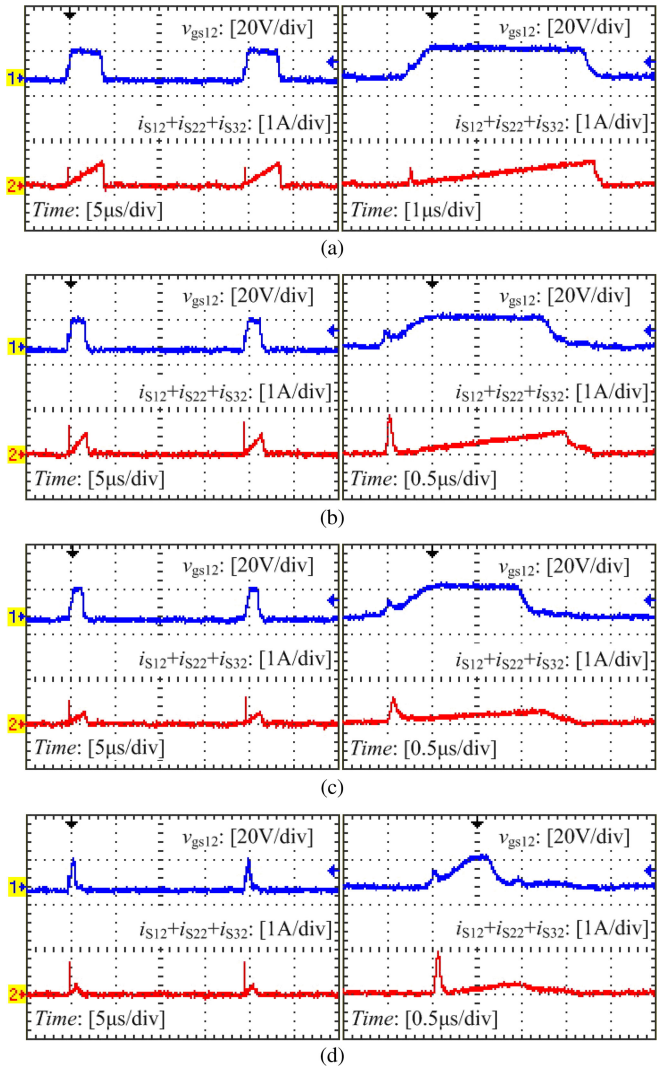

Fig. 14. Driving of S_{12} and sum current $i_{S12} + i_{S22} + i_{S32}$. (a) When $P_o = 16$ W and $V_i \approx 1050$ V. (b) When $P_o = 16$ W and $V_i \approx 2100$ V. (c) When $P_o = 3.84$ W and $V_i \approx 1050$ V. (b) When $P_o = 3.84$ W and $V_i \approx 2100$ V.

can be seen that: there is no circulating current in the sum current waveforms of $i_{S12} + i_{S22} + i_{S32}$, and this sum current is suitable to be sampled as the inner current signal of the controller.

V. Conclusion

In this paper, the circulating current problem is investigated for the input-series converters based on transformer integration. The investigation is based on this type input-series two-transistor flyback converter, mechanism and influence of the circulating current in each series module are analyzed, and according to the characteristics of its control circuit, a suppression strategy is proposed to improve the operational stability of the converter under the light load conditions. The theoretical analysis and experimental results show that: 1) the circulating current is caused by the input voltage difference of each series module, and the circulating current value will increase as the input voltage difference increases; 2) when the input voltage of the converter increases, or the conversion power of the converter decreases,

the circulating current problem becomes more serious; and 3) there is no circulating current in the sum current of various series modules, so the sum current of various series modules can be sampled as the inner current signal of the controller, by which the operational stability of this input-series converter under the light load conditions can be improved.

APPENDIX

The former analysis and verifications are aiming at the input-series two-transistor flyback converter in [31]; however, the circulating current problem also exists in the input-series single-switch flyback converter and the input-series forward converter in [30] and [32]. For the input-series single-switch flyback converter, mechanism of the circulating current when the switches are turning on is almost the same as the analysis in Section II, and the proposed suppression strategy can also be adopted. For the input-series forward converter in [32], the active IVS is realized by the forward integrated transformer, so mechanism of the circulating current may be different from that of the input-series flyback converter.

The following is the circulating current analysis of the input-series forward converter. To simplify the analysis, it is assumed that: 1) two series modules ($N = 2$) are considered; 2) the IVS process is independent of the output circuits, so only one output circuit ($n = 1$) is considered; 3) all devices are ideal, so the error of parameters in the two series modules is ignored; and 4) the output is considered as a constant voltage source due to the large output filter capacitance.

The input-series forward converter is shown in Fig. 15(a), where n_{p1}, n_{p2}, and n_{s1} ($n_{p1} = n_{p2}$) are the primary and secondary turns of the integrated transformer, and L_{f1} is the output filter inductor. During one switching period, active IVS processes of this converter also appear in two stages, in stage 1 ($t_{a0} \sim t_{a1}$), all of the switches are turning on, and the input energy is transferred to the load through the integrated transformer, and in stage 2 ($t_{a1} - t_{a2}$), all of the switches are turning OFF, and the integrated transformer operates in the magnetic-reset mode. The operational stability of this converter can be affected by the circulating current when the switches are turning ON, so the circulating current is mainly analyzed in stage 1. The equivalent circuit of this converter in stage 1 is shown in Fig. 15(b), where L_{LK1}, L_{LK2} ($L_{LK1} = L_{LK2}$) are the equivalent leakage inductance of the integrated transformer, L_{m1}, L_{m2} ($L_{m1} = L_{m2}$) are the equivalent excitation inductance, and Ti is the ideal transformer (because of $n_{p1} = n_{p2}$, it is considered that: $V_{Ti1} = V_{Ti2}$).

It is assumed that the input voltage difference (ΔV_i) appears at t_{a0}, and then the active IVS process occurs after t_{a0}. So the following relationships can be obtained before t_{a0}, $I_i = i_{p1} = i_{p2}, V_{i1} = V_{i2} = V_i/2$, and at t_{a0}, $I_i = i_{p1} = i_{p2}, V_{i1} = V_i/2 + \Delta V_i$, $V_{i2} = V_i/2 - \Delta V_i$, where $\Delta V_i(t_{a0}) > 0$. After t_{a0}, the input voltage difference can be estimated in [32] that

$$\Delta V_i(t - t_{a0}) = \Delta V_i(t_{a0}) \cos \frac{t - t_{a0}}{\sqrt{L_{LK1} C_{i1}}}. \tag{A1}$$

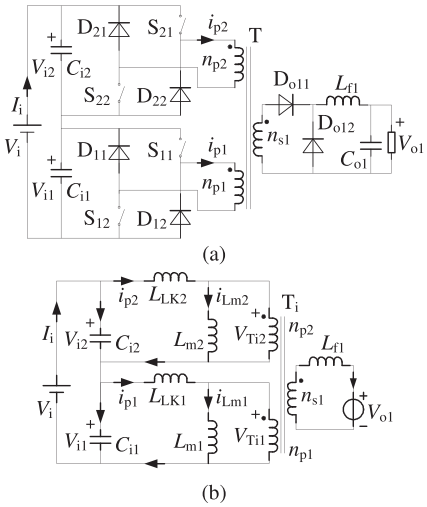

Fig. 15. Input-series forward converter. (a) Configuration ($N = 2$ and $n = 1$). (b) Equivalent circuit when the switches are turning ON (in stage 1).

It can be seen that if the input voltage difference appears at t_{a0}, a high frequency resonance will occur. Because of the internal resistance in each series module, the resonant amplitude decreases in each period, and active IVS of each series module will be achieved immediately after t_{a0}.

For the two input filter capacitors (C_{i1}, C_{i2}), it can be obtained after t_{a0} that

$$\begin{cases} C_{i1} \dfrac{dV_{i1}(t - t_{a0})}{dt} = I_i(t - t_{a0}) - i_{p1}(t - t_{a0}) \\ C_{i2} \dfrac{dV_{i2}(t - t_{a0})}{dt} = I_i(t - t_{a0}) - i_{p2}(t - t_{a0}) \end{cases} \tag{A2}$$

it can be obtained from (A2) that

$$i_{p1}(t - t_{a0}) + i_{p2}(t - t_{a0}) = 2I_i(t - t_{a0}) \tag{A3}$$

$$i_{p1}(t - t_{a0}) - i_{p2}(t - t_{a0}) = -2C_{i1} \frac{d\Delta V_i(t - t_{a0})}{dt}. \tag{A4}$$

After t_{a0}, the following relationships can also be obtained:

$$\begin{cases} L_{LK1} \dfrac{di_{p1}(t - t_{a0})}{dt} = V_{i1}(t - t_{a0}) - V_{Ti1} \\ L_{LK2} \dfrac{di_{p2}(t - t_{a0})}{dt} = V_{i2}(t - t_{a0}) - V_{Ti2} \end{cases} \tag{A5}$$

$$I_i(t - t_{a0}) = I_i(t_{a0}) + \int_{t_{a0}}^{t} \times \left[\frac{V_i}{2(L_{LK1} + L_{m1})} + \frac{V_{Ti1} - n_f V_{o1}}{2n_f^2 L_{f1}} \right] dt \tag{A6}$$

where $n_f = n_{p1}/n_{S1}$ is the turns ratio of the forward integrated transformer.

From (A3) and (A5), it can be obtained that

$$L_{LK1} \frac{dI_i(t - t_{a0})}{dt} = \frac{V_i}{2} - V_{Ti1}. \tag{A7}$$

From (A1), (A3), (A4), (A6), and (A7), the expressions of i_{p1}, i_{p2}, and I_i can be obtained

$$\begin{cases} i_{p1}(t-t_{a0}) = I_i(t-t_{a0}) + \Delta V_i(t_{a0})\sqrt{\dfrac{C_{i1}}{L_{LK1}}} \\ \qquad\qquad \sin\dfrac{t-t_{a0}}{\sqrt{L_{LK1}C_{i1}}} \\ i_{p2}(t-t_{a0}) = I_i(t-t_{a0}) - \Delta V_i(t_{a0})\sqrt{\dfrac{C_{i1}}{L_{LK1}}} \\ \qquad\qquad \sin\dfrac{t-t_{a0}}{\sqrt{L_{LK1}C_{i1}}} \end{cases} \tag{A8}$$

$$I_i(t-t_{a0}) = I_i(t_{a0}) + \int_{t_{a0}}^{t} \frac{n_f^2 L_{f1}}{2n_f^2 L_{f1} + L_{LK1}} \times \left(\frac{V_i}{L_{LK1}+L_{m1}} + \frac{V_i - 2n_f V_{o1}}{2n_f^2 L_{f1}}\right) dt. \tag{A9}$$

From the above analysis, it can be concluded that: the circulating current in the input-series forward converter is similar to that in the input-series flyback converter, which is also caused by the input voltage difference, and during the active IVS process, the varying of the input voltage difference and the circulating current can also be obtained in Fig. 4(a).

REFERENCES

[1] K T. Fang, X. Ruan, and C. Tse, "Control strategy to achieve input and output voltage sharing for input-series-output-series connected inverter systems," *IEEE Trans. Power Electron.*, vol. 25, no. 6, pp. 1585–1596, Jun. 2010.

[2] A. Bottion and I. Barbi, "Input-series and output-series connected modular output capacitor full-bridge PWM DC-DC converter," *IEEE Trans. Ind. Electron.*, vol. 62, no. 10, pp. 6213–6221, Oct. 2015.

[3] C. Song, Y. Guo, Z. Zeng, L. Sun, J. He, and M. Li, "Operation method for input-series-output parallel AC-DC-DC converter," *IET Power Electron*., vol. 9, no. 8, pp. 1654–1663, Jun. 2016.

[4] S. Chen, S. Yang, and M. Cho, "Analysis and implementation of an interleaved series input parallel output active clamp forward converter," *IET Power Electron*., vol. 6, no. 4, pp. 774–782, Apr. 2013.

[5] J. Kim, J. You, and B. Cho, "Modeling, control, and design of input-series-output-parallel-connected converter for high-speed-train power system," *IEEE Trans. Ind. Electron.*, vol. 48, no. 3, pp. 536–544, Jun. 2001.

[6] J. Kimball, J. Mossoba, and P. Krein, "A stabilizing, high-performance controller for input series-output parallel converters," *IEEE Trans. Power Electron.*, vol. 23, no. 3, pp. 1416–1427, May 2008.

[7] K. Siri, M. Willhoff, and K. Conner, "Uniform voltage distribution control for series connected DC-DC converters," *IEEE Trans. Power Electron.*, vol. 22, no. 4, pp. 1269–1279, Jul. 2007.

[8] P. Grbovic, "Master/slave control of input-series- and output-parallel-connected converters: Concept for low-cost high-voltage auxiliary power supplies," *IEEE Trans. Power Electron.*, vol. 24, no. 2, pp. 316–328, Feb. 2009.

[9] W. Chen, G. Wang, X. Ruan, W. Jiang, and W. Gu, "Wireless input-voltage-sharing control strategy for input-series output-parallel (ISOP) system based on positive output-voltage gradient method," *IEEE Trans. Ind. Electron.*, vol. 61, no. 11, pp. 6022–6030, Nov. 2014.

[10] G. Xu, D. Shang, and X. Liao, "Decentralized inverse-droop control for input-series-output-parallel DC-DC converters," *IEEE Trans. Power Electron.*, vol. 30, no. 9, pp. 4621–4625, Sep. 2015.

[11] L. Qu, D. Zhang, and Z. Bao, "Output current-differential control scheme for input-series-output-parallel-connected modular dc-dc converters," *IEEE Trans. Power Electron.*, vol. 32, no. 7, pp. 5699–5711, Jul. 2017.

[12] L. Qu, D. Zhang, and Z. Bao, "Active output-voltage-sharing control scheme for input series output series connected dc-dc converters based on a master slave structure," *IEEE Trans. Power Electron.*, vol. 32, no. 8, pp. 6638–6651, Aug. 2017.

[13] T. Fang, L. Shen, W. He, and X. Ruan, "Distributed control and redundant technique to achieve superior reliability for full modular input-series-output-parallel inverter system," *IEEE Trans. Power Electron.*, vol. 32, no. 1, pp. 723–735, Jan. 2017.

[14] W. Chen, X. Jiang, W. Cao, J. Zhao, W. Jiang, and L. Jiang, "A fully modular control strategy for input-series output-parallel (ISOP) inverter system based on positive output-voltage-amplitude gradient," *IEEE Trans. Power Electron.*, vol. 33, no. 4, pp. 2878–2887, Apr. 2018.

[15] R. Giri, V. Choudhary, R. Ayyanar, and N. Mohan, "Common-duty-ration control of input-series connected modular DC-DC converters with active input voltage and load-current sharing," *IEEE Trans. Ind. Appl.*, vol. 42, no. 4, pp. 1101–1111, Jul/Aug. 2006.

[16] Q. Lu, Z. Yang, S. Lin, S. Wang, and C. Wang, "Research on voltage sharing for input-series-output-series phase-shift full-bridge converters with common-duty-ratio," *in Proc. IEEE Annu. Conf. Ind. Electron. Soc.,* 2009, pp. 1548–1553.

[17] J. Shi, J. Luo, and X. He, "Common-duty-ratio control of input-series output-parallel connected phase-shift full-bridge DC-DC converter modules," *IEEE Trans. Power Electron.*, vol. 26, no. 11, pp. 3318–3329, Nov. 2011.

[18] A. Bottion and I. Barbi, "Input-series and output-series connected modular full-bridge PWM DC-DC converter with capacitive output filter and common duty cycle," in *Proc. 11th IEEE Int. Conf. Ind. Appl.*, 2014, pp. 1–8.

[19] S. Zong, Q. Zhu, W. Yu, and A. Huang, "Auxiliary power supply for solid state transformer with ultra high voltage capacitive driving," in *Proc. IEEE Appl. Power Electron. Conf. Expo.*, 2015, pp. 1008–1013.

[20] M. Pagliosa, R. Faust, T. Lazzarin, and I. Barbi, "Input-series and output-series connected modular single-switch flyback converter operating in the discontinuous conduction mode," *IET Power Electron*., vol. 9, no. 9, pp. 1962–1970, Jul. 2016.

[21] Q. Hu and R. Zane, "LED driver circuit with series-input-connected converter cells operating in continuous conduction mode," *IEEE Trans. Power Electron.*, vol. 25, no. 3, pp. 574–582, Mar. 2010.

[22] W. Yang, Z. Zhang, and S. Yang, "A new control strategy for input voltage sharing in input series output independent modular dc-dc converters," *J. Power Electron.*, vol. 17, no. 3, pp. 632–640, May 2017.

[23] R. Bascope and I. Barbi, "A double ZVS-PWM active-clamping forward converter: Analysis, design, and experimentation," *IEEE Trans. Power Electron.*, vol. 16, no. 6, pp. 745–751, Nov. 2001.

[24] D. Ghodke and K. Muralikrishnan, "ZVZCS, dual, two-transistor forward DC-DC converter with peak voltage of Vin/2, high input and high power application," in *Proc. 33rd Annu. IEEE Power Electron. Spec. Conf.*, 2002, pp. 1853–1858.

[25] X. Ma, W. Wang, Y. Kang, and J. Chen, "Series of two transistors forward ZVZCS converter with phase-shift control for high input voltage," in *Proc. IEEE Annu. Conf. Ind. Electron.*, 2004, pp. 761–766.

[26] D. Sha, Z. Guo, and X. Liao, "Input-series connected high frequency DC-DC converters with one transformer," in *Proc. 25th IEEE Appl. Power Electron. Conf. Expo.*, 2010, pp. 662–665.

[27] X. Song, D. Sha, and X. Liao, "Input-series common transformer connected PS-FB DC-DC converters for pulsed MIG welding," in *Proc. 27th IEEE Appl. Power Electron. Conf. Expo.*, 2012, pp. 2195–2199.

[28] S. Choi, J. Lee, and J. Lee, "High-efficiency portable welding machine based on full-bridge converter with ISOP-connected single transformer and active snubber," *IEEE Trans. Ind. Electron.*, vol. 63, no. 8, pp. 4868–4877, Aug. 2016.

[29] W. Li, Y. He, Y. Sun, F. Wang, and L. Ma, "Series asymmetrical half-bridge converters with voltage autobalance for high input-voltage applications," *IEEE Trans. Power Electron.*, vol. 28, no. 8, pp. 3665–3674, Aug. 2013.

[30] T. Meng, C. Li, H. Ben, and J. Zhao, "An input-series flyback auxiliary power supply scheme based on transformer-integration for high-input-voltage applications," *IEEE Trans. Power Electron.*, vol. 31, no. 9, pp. 6383–6393, Sep. 2016.

[31] T. Meng, Y. Song, Z. Wang, H. Ben, and C. Li, "Investigation and implementation of an input-series auxiliary power supply scheme for high-input-voltage low-power applications," *IEEE Trans. Power Electron.*, vol. 33, no. 1, pp. 437–447, Jan. 2018.

[32] T. Meng, H. Ben, Y. Song, and C. Li, "Analysis and design of an input-series two-transistor forward converter for high-input voltage multiple-output applications," *IEEE Trans. Ind. Electron.*, vol. 65, no. 1, pp. 270–279, Jan. 2018.

Tao Meng (M'15) was born in Liaoning Province, China, in 1980. He received the B.S., M.S., and Ph.D. degrees in electrical engineering from the Harbin Institute of Technology, Harbin, China, in 2003, 2005, and 2010, respectively.

He is currently an Associate Professor with the School of Mechanical and Electrical Engineering at Heilongjiang University, Harbin, China. His research interests include power factor correction techniques, high frequency ac/dc and dc/dc conversion techniques, magnetic integration technique and its applications.

Hongqi Ben was born in Heilongjiang Province, China, in 1965. He received the B.S. degree in electrical engineering from the Shenyang University of Technology, Shenyang, China, in 1988; the M.S. degree in electrical engineering; and the Ph.D. degree in mechanical engineering from the Harbin Institute of Technology, Harbin, China, in 1991 and 1999, respectively.

He is currently a Professor with the School of Electrical Engineering and Automation at Harbin Institute of Technology, Harbin. His research interests include high frequency power conversion techniques and power factor correction techniques.

Yilin Song was born in Shandong Province, China, in 1960. He received the B.S. degree in mechanical engineering from Tongji University, Shanghai, China, in 1982; the M.S. degree in mining machinery from the University of Science and Technology Beijing, Beijing, China, in 1987; and the Ph.D. degree in division of innovative technology and science from Kanazawa University, Jinze, Japan, in 2002.

He is currently a Professor with the School of Mechanical and Electrical Engineering at Heilongjiang University, Harbin, China. His research interests include theory and application of mechatronics.

Chunyan Li was born in Heilongjiang Province, China, in 1980. She received the B.S. degree in automation from Heilongjiang University, Harbin, China, in 2003; the M.S. and Ph.D. degrees in electrical engineering from Harbin Institute of Technology, Harbin, China, in 2005 and 2010, respectively.

She is currently an Associate Professor with the School of Mechanical and Electrical Engineering at Heilongjiang University, Harbin. Her research interests include the design and control of permanent magnet motors.